NANO LETTERS

Letter

pubs.acs.org/NanoLett

Single Layer Molybdenum Disulfide under Direct Out-of-Plane Compression: Low-Stress Band-Gap Engineering

Miriam Peña-Álvarez,[†,‡] Elena del Corro,*[,†] Ángel Morales-García,[§] Ladislav Kavan,[†] Martin Kalbac,[†] and Otakar Frank*[,†]

[†]J. Heyrovsky Institute of Physical Chemistry of the AS CR, v.v.i., Dolejskova 2155/3, 182 23 Prague 8, Czech Republic

[‡]Departamento de Química Física I, Facultad de Ciencias Químicas, Universidad Complutense de Madrid, Madrid 28040, Spain

[§]Department of Physical and Macromolecular Chemistry, Faculty of Science, Charles University in Prague, Hlavova 2030, Prague 2, 128 43, Czech Republic

Supporting Information

ABSTRACT: Tuning the electronic structure of 2D materials is a very powerful asset toward tailoring their properties to suit the demands of future applications in optoelectronics. Strain engineering is one of the most promising methods in this regard. We demonstrate that even very small out-of-plane axial compression readily modifies the electronic structure of monolayer MoS_2. As we show through in situ resonant and nonresonant Raman spectroscopy and photoluminescence measurements combined with theoretical calculations, the transition from direct to indirect band gap semiconductor takes place at ∼0.5 GPa, and the transition to a semimetal occurs at stress smaller than 3 GPa.

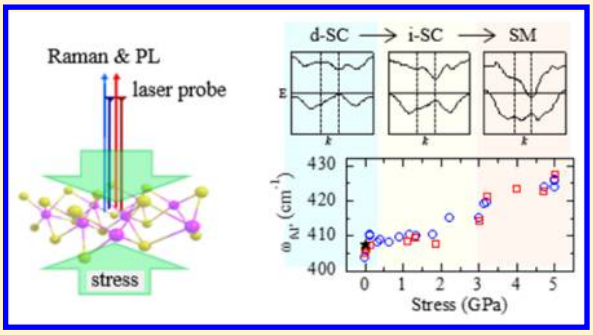

KEYWORDS: *Molybdenum disulfide, band gap engineering, out-of-plane compression, anvil cell, Raman spectroscopy, electronic properties calculations*

Starting with the preparation of graphene, the whole family of two-dimensional (2D) materials has been attracting a steady increase in popularity owing to their exceptional mechanical and optoelectronic properties, which are often dramatically different from the properties of their bulk progenitors.[1,2] Moreover, those exceptional properties can be further tuned externally, for example, by doping,[3] functionalization,[4] or strain,[5] thereby opening pathways to a vast array of possible applications.[2,6,7] Apart from graphene, transition metal dichalcogenides (TMDs), and molybdenum disulfide (MoS_2) in particular, belong to the 2D materials family.[4] Bulk MoS_2 is a 1.3 eV indirect band gap semiconductor, while its monolayer (1L) constituent has a direct band gap of 1.9 eV.[8] The effective Young's modulus of 1L-MoS_2 measured by AFM indentation is 270 ± 100 GPa[9] (or 330 ± 70 GPa for few layer MoS_2).[10] The high strength and elasticity predestines the electronic structure of MoS_2 (and similar 2D materials) to be tuned by mechanical deformation to a large extent, finding potential utilization, for example, in light harvesting through funneling[11] or photocatalysis.[12]

Recently, numerous works appeared demonstrating the strain engineering of 1L-MoS_2 experimentally and/or theoretically,[13−28] pointing to the crucial importance that the strain direction may have on both the absolute band gap energy and the sign of its change with progressive deformation. It should be noted that in specimens with two or more layers the strain-tuning gains another degree of freedom through the modification of interlayer coupling.[29−35] Small uniaxial strains (up to 2% of tension) were applied to monolayer and bilayer MoS_2 via bending of their polymeric substrates.[14,19,26,28] Under these conditions, the direct optical gap of 1L-MoS_2 red-shifted alongside with the bleaching of the intensity of the corresponding photoluminescence (PL) band, and the transition to an indirect band gap took place at ∼1.3% of strain.[14] An increase of the band gap energy was observed during the application of biaxial in-plane compression (accompanied by out-of-plane Poisson tension) of trilayer MoS_2.[33]

The effect of hydrostatic pressure on bulk and 1L-MoS_2 has been recently reported. In the case of single layered samples, the direct band gap energy of 1L-MoS_2 was shown to increase[15,24] and the transition from direct to indirect band gap appeared at ∼23 GPa, as estimated from the disappearance of the A peak in the PL spectrum along with theoretical calculations, while the semiconductor−semimetal transition is predicted to happen at ∼68 GPa.[24] For bulk MoS_2 under hydrostatic compression, a previous work, combining Raman spectroscopy and in situ resistivity measurements, claimed that hydrostatic conditions tuned the electronic properties of the bulk material leading to the semiconductor to semimetal

Received: January 20, 2015
Revised: April 13, 2015
Published: April 27, 2015

ACS Publications © 2015 American Chemical Society

DOI: 10.1021/acs.nanolett.5b00229
Nano Lett. 2015, 15, 3139−3146

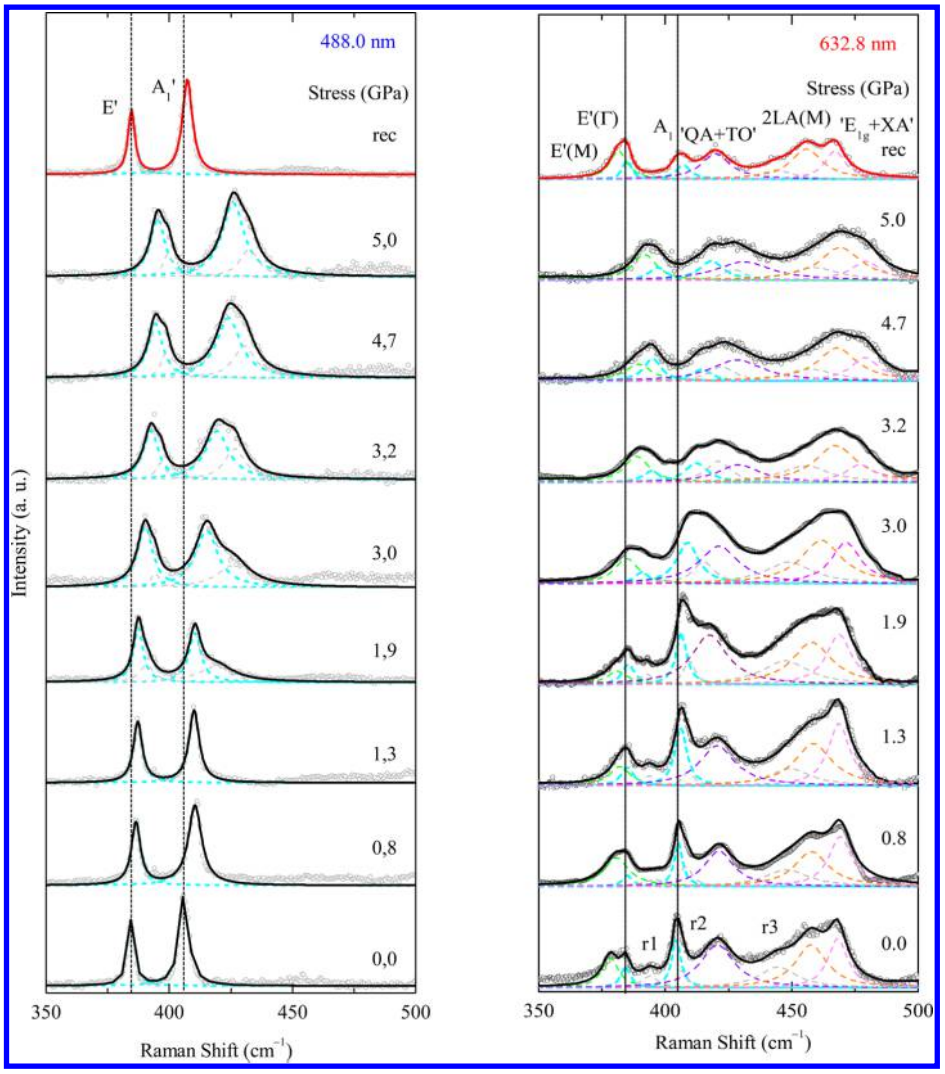

Figure 1. Raman spectra of 1L-MoS_2 under axial compression (with stress indicated for every curve; "rec" stands for recovered), registered with the (a) 488.0 and (b) 632.8 nm laser excitation wavelengths. Colored dashed lines represent the fitted Lorentzian contributions with the solid curves representing their sum. Spectra are offset for clarity and normalized to the E′ band.

electronic transition, via an intermediate state. The pressures at which the electronic transitions took place are 10 and 19 GPa, respectively.[31] Also for the bulk system, high pressure experiments have been carried out together with diffraction analysis. First, Aksoy et al.[36] showed the evolution of the *a* and *c* lattice parameters and observed abrupt discontinuities at ∼20 GPa.[36] Later on, it was confirmed by Chi et al.[37] that bulk MoS_2 under hydrostatic pressure shows a structural transition from the 2Hc to the 2Ha phase at 20 GPa, hence in the range of the semiconductor−metal transition observed by Nayak et al.[31] In view of these previous results, one can assume that the metallization of MoS_2 is accompanied by a structural transition within the same crystal symmetry.

In this Letter, we demonstrate a very efficient mechanical experiment that can be successfully utilized to modify the electronic structure of monolayer MoS_2, the anvil cell experiment without the presence of a pressure transmitting medium, thereby exerting uniaxial out-of-plane compression. As shown experimentally, through in situ monitoring by both resonant and nonresonant Raman spectroscopy and PL measurements, as well as theoretically, the electronic structure of MoS_2 is extremely susceptible to the changes of the atom positions within a single MoS_2 sheet. The transition from direct to indirect band gap semiconductor takes place immediately after closing the anvil cell when the stress is increased ∼0.5 GPa, while the metallization (to a semimetal) occurs at stress as low as 2.8 GPa. The direct−indirect transition is fully reversible, whereas after reaching the semimetal nature the MoS_2 does not return to its original state even after the stress release; it remains as an indirect gap semiconductor indicating not fully elastic behavior after crossing over the semiconductor−semimetal transition. Furthermore, a thorough density functional theory (DFT) study was performed to compare the effects of both hydrostatic and normal uniaxial stress exerted on monolayer as well as on bulk MoS_2.

Single layer MoS_2 samples were axially compressed in the out-of-plane direction in various anvil cell configurations. The particular set-ups were chosen depending on the purpose of the measurement, that is, Raman spectroscopy or PL or both (but with severe limitations in the latter case). For details on the samples and set-ups, see Methods and also Figures S1−S3 (Supporting Information). Figure 1 shows the evolution of the Raman spectrum of single layered MoS_2 with the increasing out-of-plane axial stress, registered with two different excitation

DOI: 10.1021/acs.nanolett.5b00229
Nano Lett. 2015, 15, 3139−3146

wavelengths, 488.0 nm (2.54 eV) and 632.8 nm (1.96 eV). At ambient conditions (Figure 1, bottom), the Raman spectrum of 1L-MoS_2 shows quite a different profile depending on the laser energy used for the sample excitation. It has been observed that for excitation energies around 2 eV (close to the energy of excitons A and B)[38] a number of additional Raman features, apart from the well-known normal modes E′ and A_1', can be detected.[39−41] For the 488.0 nm laser excitation, the resonance conditions are not fulfilled and the Raman spectrum is governed by the first-order modes (Figure 1 left), whereas the resonant Raman spectrum is observed with the 632.8 nm excitation wavelength (Figure 1 right). The second-order Raman spectrum of 1L-MoS_2 has been measured previously,[39,42−44] and the origin of many of these additional contributions is still a subject of discussion.

In Figure 1 we use the reported notation for the bands around 378 cm^{-1} (E′(M)), 421 cm^{-1} ("QA + TO"), 453 (2LA(M)) and 467 cm^{-1} ("E_{1g} + XA"), taken from refs 39, 40, 42, and 45, however an alternative assignment for some of these bands has arisen recently.[44] Specifically, Livneh and Spanier[44] propose an alternative assignment for the band at 421 cm^{-1} (which is discussed later on) and state that in the 450−470 cm^{-1} spectral range, there are in fact more than two contributions, all of them belonging to LA phonons at and in between the M and K points. Several other weaker contributions can be observed, labeled here as r1, r2, and r3 (in gray in Figure 1 right). Note that we do not use the common a, b, c notation because the particular designation of those bands tends to differ in the literature.[35,39,40] For example, the r1 band is observed (but not fitted) in ref 39, while the same contribution is denoted as the "a" band in ref 35 and its origin has just been assigned to the combination "$A_1(\Gamma)$ + $E(M_2)$".[44] On the other hand, the frequency of this band coincides with the E_{1u} Raman-inactive phonon of bulk MoS_2,[46] which could be also visible in the resonant Raman spectrum. The band, denoted as r2, is not clearly discernible in the pristine sample due to its proximity to the A_1' band. This band was observed previously in the Raman spectra of MoS_2 nanoparticles with particular sizes.[42] Here, the stress treatment allows us to distinguish this contribution, which, accordingly to its position, might be attributed to the A_1' phonon in the vicinity of the M point of the Brillouin zone, analogously to the E(M) band at 378 cm^{-1}.[39] Finally, in our spectra the 2LA(M) band shows a shoulder at lower frequency, which we fitted by adding an additional contribution, r3. Recently, this contribution was assigned to the combination band "A_{1g} (Γ) + E^2_{2g} (Γ)",[44] which is in agreement with our study, because we might assign the r3 contribution to an out-of-plane vibration due to its larger axial stress coefficient compared to that of the 2LA(M) band, 6.3 versus 3.5 cm^{-1}/GPa, respectively, or to that of the normal modes (reported later on).

At a first glance, Figure 1 shows that, as expected, the whole spectrum upshifts and broadens with increasing stress. Under nonresonant conditions only the E′ and A_1' bands are observed but interestingly new contributions arise for stresses around 2 GPa on the high frequency sides of the E′ and A_1' bands. These new contributions cannot be clearly distinguished in the 632.8 nm spectra due to the high intensity of the second-order features under resonant conditions; however, their presence cannot thus be ruled out either. For a deeper insight of the changes under stress, the spectra are analyzed as a sum of Lorentzian contributions, also depicted in Figure 1.

The peak position of the normal modes as a function of the stress is presented in Figure 2a for the two employed laser

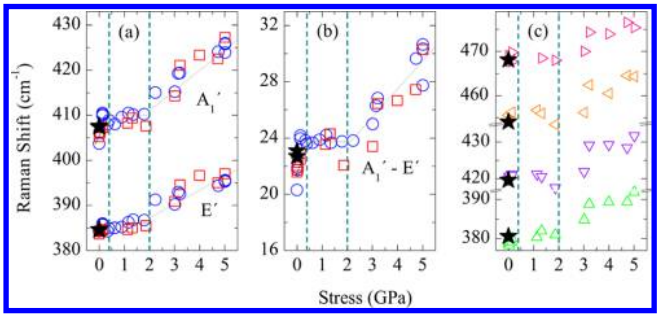

Figure 2. (a) Raman shift of the E′ and A_1' bands and (b) frequency difference as a function of applied stress. Red squares and blue circles stand for the 632.8 and 488.0 nm spectra, respectively. (c) Raman shift as a function of applied stress of the second-order bands measured with the 632.8 nm excitation energy: E′(M) (green), "QA + TO" (magenta), 2LA(M) (yellow), and "E_{1g} + XA" (pink). Values corresponding to the recovered samples are depicted by black stars. Dashed vertical lines indicate the stress thresholds of the electronic phase transitions. Solid lines in (a) and (b) are the linear least-squares fits of the evolutions of the first-order bands in individual stages.

excitation energies. Obviously, the trend of the evolution of the first-order modes with stress is the same regardless the resonance conditions. For both excitations, the experimental data points in Figure 2a can be assigned to three regions with particular stress behaviors. With slight compression at around 0.5 GPa, the E′ and A_1' modes suddenly upshift approximately by 2 and 5 cm^{-1}, respectively. However, when the stress is continuously built up to 2 GPa, the frequencies of the normal modes remain almost unaltered. Finally, if the stress is increased beyond this value, up to 5 GPa, the E′ and A_1' bands upshift again, with coefficients of 2.8 and 5.0 cm^{-1}/GPa, respectively. The higher sensitivity of the A_1' mode is expected due to its out-of-plane origin. Figure 2a shows data from two kinds of experimental setups, the sample on a sapphire and on an Inconel substrate directly opposed to a sapphire or a moissanite anvil, respectively. It is interesting to note that the three-region behavior observed is not influenced by the substrate, even when using quite different materials in terms of both hardness and dielectric properties.

A three-region behavior is also observed for the frequency difference ($\omega_{A1}' - \omega_{E}'$) and for the second-order bands as a function of stress, Figure 2b,c. Such results resemble the behavior found for bulk MoS_2 under hydrostatic pressure but with different stress thresholds.[31] Obviously, both the studied system and the stress conditions are different in our experiment compared to ref 31, monolayer under axial versus bulk in hydrostatic; therefore, it is difficult to compare the results directly. However, the perfect resemblance of the evolution of the Raman first-order modes in both experiments allows us to assume that the nonlinear behavior of the E′ and A_1' bands is indeed correlated with electronic transitions, namely the change at ∼0.5 GPa would be related to the direct−indirect band gap semiconductor transition and the change at ∼3 GPa to the semiconductor−semimetal transition. Moreover, analogous nonlinearities in the evolution of the E′ band were also discerned in the region of direct−indirect gap transition when subjecting 1L-MoS_2 to in-plane tensile strain.[26]

The relationship between the different Raman trend with stress and the electronic state is still an open question. One

DOI: 10.1021/acs.nanolett.5b00229
Nano Lett. 2015, 15, 3139−3146

might think that the exciton−phonon (e-p) coupling could play a role, because a number of studies prove the influence that the e-p coupling has on the Raman spectrum of TMDs.[35,42,47] Therefore, the different Raman trends could be governed by changes in the e-p coupling, as a consequence of the modifications of the electronic structure induced by the stress increase. For example, unexpected changes in the intensity of the A_{1g} mode in bulk MoS_2 with hydrostatic pressure have been observed and preliminarily ascribed to varying interaction of the phonons with the changed electronic structure by Livneh et al.[35] In the case of the indirect semiconductor to semimetal transition, one should also consider the possibility of a simultaneous structural change under stress (analogous to the one observed in bulk samples[36,37]), which could explain the different evolution of Raman peaks in accordance with a change of lattice parameters. Finally, our theoretical calculation predicts a small but clearly visible sudden change in the compressibility of 1L-MoS_2 at ∼3 GPa, that is, at the point of metallization, see Figure S10 (Supporting Information). The rate of decrease of the S−S distance with stress changes there from ∼−0.156 to ∼−0.183 Å/GPa. It is assumed that such a change can contribute to the change in the A_1' shift rate as well.

We now turn our attention to the new Raman bands emerging at ∼390 and ∼419 cm^{-1} in the 488.0 nm excited spectra at stress around 2 GPa (Figure 1 left). Interestingly, a new unassigned band at the high frequency side of E′ was observed previously in bulk MoS_2 under 19 GPa of hydrostatic pressure.[35] We note that at a similar pressure (∼20 GPa), the transition from an indirect gap semiconductor to a metal was reported for bulk MoS^2.[31] Thus, there seems to be a reasonable correlation between the appearance of this band at ∼390 cm^{-1} and the mentioned electronic transition, also in our case. The frequency of this new band is the same as that of the r1 band, therefore, this band might be assigned to the E_{1u} mode, which becomes Raman active under nonresonant conditions as a consequence of the perturbations imposed on the lattice, for example, experienced by the sample in the semiconductor to semimetal transition.

Regarding the band at ∼419 cm^{-1}, one can be tempted to assign it to the QA + TO band, which appears also in the Raman spectra excited by the 632.8 nm laser (Figure 1 right). Sekine et al.[45] proposed that this band can be attributed to a two-phonon Raman process involving a successive emission of a dispersive longitudinal quasi-acoustic (QA) phonon and a dispersionless TO phonon along the *c*-axis. The frequency of the peak can be not only tuned in dependence on the excitation energy, it is also related to the relative energy separation between the incident photon and either the 1s level of the A exciton or the 1s level of the B exciton.[45] Furthermore, the Raman cross-section of this peak is also highly dependent on the excitation energy.[45] It can be assumed that upon the application of stress in 1L-MoS_2 and the subsequent changes of its electronic structure, this particular peak can appear also in Raman spectra excited by a laser of a shorter wavelength, because the incident photon got closer to the exciton B energy. It was shown that the shift rate of the QA + TO band with 632.8 excitation under hydrostatic pressure resembles the behavior of the A_1' peak because of the composite effect of the tuning of the A exciton energy with stress and the strain dependence of the phonon.[35] However, in an earlier work the exciton B energy was shown to increase at a faster rate compared to the exciton A energy.[48] Hence, the possibility of appearance of this peak in spectra excited by a higher energy laser cannot be ruled out. This hypothesis is also supported by the gradual increase of the intensity of this peak in the measured stress range (see Figure S5, Supporting Information), a behavior substantially different to all other analyzed Raman bands in the spectra. An alternative explanation about the origin of the QA + TO band has been recently given, showing it is in fact separated into two peaks, for which the combinations of acoustic phonons at K ("LA(K) + TA(K)" and "LA(K) + ZA(K)") can be considered.[44] As has been shown, these two peaks are visible also in Raman spectra excited by 1.58 eV laser (i.e., nonresonant), however, their relative intensities differ from those measured using a resonant excitation. Also, in this case it could be assumed that upon the application of stress connected with the change of exciton energy, the resonance conditions of the peaks will vary and one of them (or both) may become dominant in the spectra.

Concerning the full width at half-maxima (fwhm), presented in Figure 3, two plateaus can be observed as a function of the stress, for all the analyzed Raman features, with the exception of the QA + TO combination band. The fwhms of the Raman contributions remain unaltered with increasing stress up to 2 GPa, when the semiconductor to semimetal transition occurs; at this stress value the widths suddenly increase, to remain constant again as the compression proceeds. In the case of the QA + TO band, its fwhm is unchanged only at the very earliest compression stage (up to about 0.5 GPa), but it increases continuously for almost the whole stress range. This observation can be in line with the proposed assignment of the band to a two-component feature coming from the acoustic phonons at K, where the individual peaks shift at different rates with stress, thereby increasing gradually the fwhm of their sum.

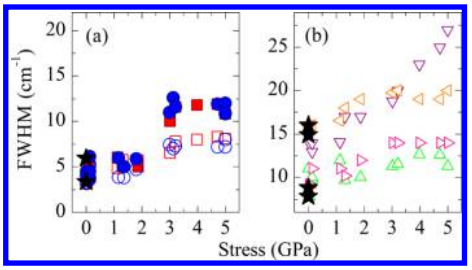

Figure 3. (a) The fwhms as a function of applied stress of the E′ and A_1' bands, empty and filled symbols, respectively. Red squares and blue circles correspond to the 632.8 and 488.0 nm spectra, respectively. (b) The fwhms as a function of applied stress of the second-order bands (measured with the 632.8 nm line): E′(M) (green), QA + TO (magenta), 2LA(M) (yellow), and E_{1g} + XA (pink). Values corresponding to the recovered samples are depicted by black stars.

For systems analogous to MoS_2 it has been shown that resonant Raman spectroscopy can provide information about the electronic properties,[49] because the intensity of the Raman spectrum is enhanced when the excitation energy coincides with the energy difference between two electronic states. Therefore, the electronic transitions described here would imply changes in the resonance conditions, which in turn should be reflected in the intensity of the Raman spectrum. The intensity (area) evolution with stress of the main Raman contributions in the 632.8 nm spectra is presented in Figure S4 (Supporting Information). We can clearly observe a decrease of intensity for all the Raman contributions presented at stresses ∼3 GPa, indicating a change in the resonance conditions due to

DOI: 10.1021/acs.nanolett.5b00229
Nano Lett. 2015, 15, 3139−3146

the electronic transition described (semiconductor to semimetal).

Complementary photoluminescence experiments have been carried out in order to probe the electronic changes announced by Raman spectroscopy. First, a 1L-MoS_2 sample was compressed up to 1 GPa, so that only the direct−indirect semiconductor transition was achieved but not yet the semimetal phase. Second, the same recovered sample is subjected to a second stress cycle, reaching a maximum stress of 3 GPa, slightly higher than the stress threshold for the transition to semimetal. In both stress cycles, we performed simultaneous Raman and photoluminescence measurements on both the compressed and recovered samples, which are shown in Figure 4, compared with that of the pristine material. The

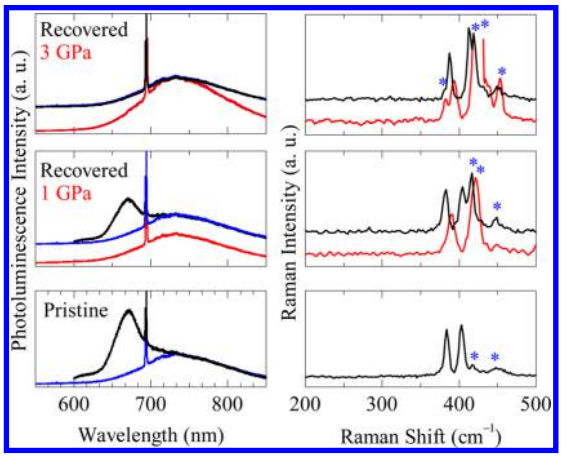

Figure 4. Photoluminescence (left) and Raman (right) spectra of a pristine 1L-MoS_2 and the compressed and recovered sample after 1.0 and 3 GPa compressions. Black spectra correspond to the nonstressed samples and red spectra to the compressed ones. Sapphire substrate spectra is presented in blue and indicated by asterisks.

prominent photoluminescence peak of 1L-MoS_2 appears at 671.3 nm (1.85 eV), which is in agreement with previous studies.[8] Note that the effect of the substrate and the influence of doping level on the PL signal of 1L-MoS_2 has been recently reported,[50−53] revealing some differences in the shape and position of the A peak, when comparing with differently supported samples. In our case, the PL spectrum of sapphire-supported 1L-MoS_2 coincides with that of Si/SiO_2 samples (see the PL spectrum of 1L-MoS_2 on Si/SiO_2 in Supporting Information Figure S7).

We observe that as soon as we start compressing the sample the photoluminescence is quenched and no signal can be distinguished from the sapphire background (blue dashed line in Figure 4). When the sample is released, the photoluminescence signal is partially recovered and quenched again with increasing stress up to 3 GPa. At such stress level, the transition to semimetal has already occurred, and once more the photoluminescence peak of MoS_2 is not observed. The corresponding Raman spectra show no additional peaks associated with defects, especially the peak corresponding to the LA(M) phonon (at ~223 cm^{-1}),[40,42] so we can assume that the stress treatment is not generating disorder in the samples, hence a disorder is not the cause of the photoluminescence signal vanishing. Moreover, the main Raman peaks of the downstroke measurement mostly recover their original fwhm values (see black stars in Figure 3); also disregarding the creation of defects[54] during the stress treatment, and their implication in the observed photoluminescence changes. The nonreversibility of the transformation once the semimetallic phase is achieved is also visible in the corresponding Raman spectra. While the frequencies of the normal modes in the downstroke sample after 1 GPa stress loading recover their original values in the case of the recovered sample after 3 GPa compression the A_1' band remains slightly up,shifted (by approximately 3 cm^{-1}). This is also observed in the recovered sample after 5 GPa compression (see stars in Figure 2a). Because only the out-of-plane A_1' mode remains slightly upshifted and broaden, one can assume that the recovered sample (from the semimetal state) presents no residual strain along the plane but its sulfur layers stay slightly constrained against each other. Such nonreversibility could be caused by an interaction with the substrate (mainly affecting the out-of-plane vibrations), being enhanced under extreme stress and not fully reversible.

Theoretical calculations have been carried out in order to investigate the electronic transitions described on the basis of the Raman results. For this purpose, the electronic structure of a single layer of MoS_2 is calculated as a function of increasing stress. First, the electronic structure of the unstrained sample is obtained; as presented, it shows a direct band gap at the K point of the Brillouin zone of 1.81 eV, which is in agreement with previous studies.[8,55] The gap between the conduction band at K and the valence band at Γ is larger in the unstrained sample (2.00 eV); however, the evolution of the electronic structures with the increasing axial stress (shown in Figure 5) reveals a transition from direct to indirect band gap semiconductor at around 0.6 GPa. This result is in excellent agreement with the results obtained in our PL measurements in which we observed the vanishing of the PL signal as soon as the

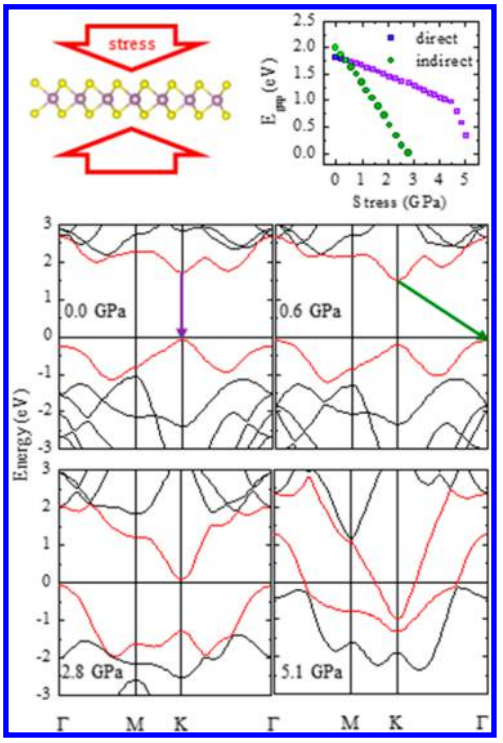

Figure 5. Theoretical calculations of the electronic structure of 1L-MoS_2 under compression. Evolution of the direct and indirect band gap energies with stress.

DOI: 10.1021/acs.nanolett.5b00229
Nano Lett. 2015, 15, 3139−3146

cell was closed (i.e., around 0.5 GPa). From this stress value onward, the valence band maxima (VBM) and conduction band minima (CBM) continue converging with compression (see Supporting Information for a complete stress sequence). At 2.8 GPa, we can observe that both the VBM at the Γ point and the CBM at the K point are at the Fermi level, indicating the transition to a semimetal phase, which is in good agreement with our Raman spectroscopy observations. Under hydrostatic pressure, the same transition was observed in the bulk at 23.8 GPa[31] and predicted to take place at 68 GPa in 1L-MoS_2.[24] The smaller stress needed (0.5 and 3.0 GPa) to reach the direct−indirect gap transition and the semiconductor−semimetal transition in our type of experiment (compared to hydrostatic pressure or to in-plane tensile strains) evidence a very high sensitivity of the monolayer MoS_2 to the changes in the position of the atoms.

This large disparity in the response to seemingly very similar stress modes (normal uniaxial versus hydrostatic) can be explained by a deeper look into the evolution of both crystal and electronic structure exposed to the particular deformation type. First, we compare the bulk MoS_2 under the two compression regimes (Figures S11, top, and S12 and the related discussion in Supporting Information). Interestingly, the response of the electronic structure is very similar in both regimes, namely a gradual decrease of the band gap energy despite different trends of rearrangement of the atoms within individual layers. However, these intralayer changes are in both cases small compared to a fast decrease of the interlayer distance (hence increase of the interlayer interactions), which thus seems to be crucial in the electronic structure modification. On the other hand, the behavior of 1L-MoS_2 is entirely different: the CBM moves down in energy and remains at the K point under uniaxial stress, while it moves up in energy and also changes from K to Q (a lower symmetry point between K and Γ) under hydrostatic compression (Figure S11, bottom, Supporting Information). The changes in VBM are smaller, its position swaps from K to Γ under uniaxial, while it stays (at least initially) at K under hydrostatic conditions. As a result, for an axially compressed sample the quickly emerging indirect band gap is K-Γ and is gradually reduced. In contrast, the indirect band gap takes over at higher hydrostatic pressures and it happens between the Q and K states. Furthermore, Figure S13 (Supporting Information) documents the gradual increase of hydrostatic stress needed to achieve the same level of normal compression as the axial one does, which also accounts for the observed differences in the onset of electronic transitions.

Additionally, we studied the evolution of Mo−S bonds in terms of the electron localization function (ELF). At 0 GPa, the Mo−S bond has a strongly ionic character with a small covalent participation. With the increasing out-of-plane axial stress, the bonding character is shifted steadily toward covalent. For more details, see Figure S7 and the related description (Supporting Information). Moreover, the ELF at 5 GPa confirms the absence of any S−S bonding across the MoS_2 layer.

In summary, we have demonstrated that the application of small out-of-plane axial stress in anvil cells without pressure transmitting media can be used for strain engineering of the electronic structure of monolayer MoS_2. The transition from direct to indirect band gap semiconductor takes place immediately after the cell assembly, at ∼0.5 GPa, followed by a transition to a semimetallic state between 2 and 3 GPa. The changes were monitored by in situ Raman spectroscopy, using both resonant (632.8 nm) and nonresonant (488.0 nm) laser excitation wavelengths, together with photoluminescence measurements. The experimental data are in an excellent agreement with DFT calculations of the electronic structure. The first transition (direct-indirect semiconductor) is accompanied by a full photoluminescence quenching and a sudden change of the evolution of the first-order Raman peaks. This transition is fully reversible. The second transition (semiconductor-semimetal) is reflected in another abrupt change of the Raman peak shifts and is not completely reversible−the A_1' frequency differs by approximately 2−3 cm^{-1} from the original positions and the PL is not recovered. However, based on the analysis of the Raman peak widths and the absence of defect-related Raman bands throughout the whole experiment, no irreversible disorder is induced upon the compression. A structural transition, though without changing the overall symmetry of the material, can be responsible for the observed effect.

Methods. *Anvil Experiments.* The MoS_2 samples investigated here were prepared from commercial MoS_2 (SPI) by the mechanical exfoliation method. First, the samples are placed on a freshly cleaned 300 nm SiO_2/Si substrate and characterized by optical microscopy, atomic force microscopy (AFM), and Raman spectroscopy.[56] Then, the monolayer samples were transferred,[57] depending on the experiment, to a sapphire disc (2 mm thick and 10 mm diameter, from UQG Optics) or to an Inconel disc (see Supporting Information). Optical and AFM images were measured after transfer to confirm that the sample remained unaltered after its manipulation. For the Raman measurements, a moissanite anvil cell was used and the sample, placed on a nondrilled Inconel disc, was positioned between the two anvils without any pressure transmitting medium. Additionally, we prepared a cell consisting of a sapphire anvil opposed to a sapphire disc containing the sample. In such configuration, one of the intense Raman features of sapphire overlaps with the A_1' band of MoS_2, thus hindering its precise measurement. Thus, only a limited set of data could have been obtained under this setup, which, however, confirmed the behavior observed in the Inconel samples. For the photoluminescence measurements, we used a moissanite anvil opposed to a sapphire disc. This device allowed us to measure the photoluminescence spectrum, avoiding the possible quenching of the signal due to the Inconel metal but adding the photoluminescence of the sapphire background to our measurements. In none of these high pressure setups could the conventional stress markers be used, as it would cause bridging between the anvils. As already done in other cases in the literature,[58] we used the Raman shift of the anvil as stress sensor. In our experiments, we use the reported stress coefficients of moissanite,[59] which provide an accuracy in the stress estimation of ±0.5 GPa.

Characterization. Raman and photoluminescence measurements were performed using a LabRAM HR spectrometer (Horiba Jobin-Yvon) using the 1800 and 600 grooves mm^{-1} gratings. For the sample excitation, we used an Ar/Kr laser (488.0 nm) and a He/Ne laser (632.8 nm). A 50× objective was used, providing a laser spot of about 1 μm in diameter. The laser power on the sample was kept below 0.5 mW to avoid sample damage. AFM images were recorded using a Dimension Icon Microscope (Bruker) with ScanAsyst-Air tips in the PeakForce tapping mode.

First-Principles Calculations. The electronic structure calculations of unstrained and strained monolayer MoS_2 were performed using first-principles DFT based methodology, as

DOI: 10.1021/acs.nanolett.5b00229
Nano Lett. 2015, 15, 3139−3146

implemented in the Vienna Ab initio Simulation Package (VASP) package.[60] All-electron projector augmented wave (PAW) pseudopotentials[61,62] represent the core electrons, while the valence electrons are explicitly treated using plane waves of cutoff 420 eV. The Perdew, Burke, and Ernzerhof (PBE-GGA) functional[63] is used to solve the Khon-Sham equations; analogous approximation was used in a recent study[31] concerning the properties of bulk MoS_2. A well-converged Monkhorst and Pack *k*-points set ($12 \times 12 \times 1$) was used for the Brillouin zone sampling.[64] The optimization of the lattice parameters was completed using the primitive unit cell of bulk MoS_2. The calculated values of *a* (3.18 Å) and *c* (13.99 Å) are close to other reported theoretical[16] and experimental results.[65] Then, to simulate a single layer, a vacuum of approximately five layers was introduced to avoid interaction between periodic images of slabs in the *z*-direction.

For the subsequent strained configurations, the S−S distance was decreased along the *z*-direction and the Mo atoms were allowed to relax, keeping the *a* and *c* lattice parameters constant. The equivalent stress acting on the cell is obtained for both directions *z* and *x* (=*y*). The ratio between the in-plane and out-of-plane stress is in good agreement with previous experimental results using moissanite anvil cells.[59] The out-of-plane (*z*) stress values depicted in this work are multiplied by a factor considering the relation between the unit cell top surface and the real section occupied by the atoms in the cell. The so-obtained stress values coincide with those calculated as the energy cost over the cell volume (taking the S−S distance as the *c*-parameter in the monolayer system).

■ ASSOCIATED CONTENT

Supporting Information

Photographs and AFM image of the 1L-MoS_2 flake. Schematic representation of the anvil cell configurations used for the different characterization techniques. Analysis of the evolution of the Raman intensities with stress for the most prominent features in the 632.8 nm spectra. Analysis of the extra bands (in gray in Figure 1). Photoluminescence spectra of Si/SiO_2 and sapphire supported samples and of the different gem anvils. Calculated electronic structure evolution under high stress (complete sequence form 0 to 5 GPa). Electron localization function at 0 and 5 GPa. Computational comparative study of bulk and single layered MoS_2 under different stress conditions. The Supporting Information is available free of charge on the ACS Publications website at DOI: 10.1021/acs.nanolett.5b00229.

■ AUTHOR INFORMATION

Corresponding Authors

*E-mail: (E.d.C.) edelcorro@quim.ucm.es.
*E-mail: (O.F.) otakar.frank@jh-inst.cas.cz.

Author Contributions

The manuscript was written through contributions of all authors. All authors have given approval to the final version of the manuscript.

M.P.A. and E.d.C. contributed equally.

Notes

The authors declare no competing financial interest.

■ ACKNOWLEDGMENTS

This work was funded by Czech Science Foundation project No. 14-15357S. M.K. and E.d.C. acknowledge the support from ERC-CZ project No. LL1301. The authors also acknowledge support from the Spanish Ministry of Economy (CTQ2012-38599-C02-02). M.P.A. is grateful to the Spanish Ministerio de Educación, Cultura y Deporte for an FPU grant and to the European Community for an Internship Erasmus grant. A.M.-G. acknowledges financial support through the Seventh Framework Programme of the European Union (FP7/2007-2013). MALTA-HPC computing center is also acknowledged. We also thank Professor Valentín García Baonza and Mercedes Taravillo for useful discussions.

■ REFERENCES

(1) Novoselov, K. S.; Jiang, D.; Schedin, F.; Booth, T. J.; Khotkevich, V. V.; Morozov, S. V.; Geim, A. K. *Proc. Natl. Acad. Sci. U.S.A.* **2005**, *102*, 10451.
(2) Butler, S. Z.; Hollen, S. M.; Cao, L.; Cui, Y.; Gupta, J. A.; Gutiérrez, H. R.; Heinz, T. F.; Hong, S. S.; Huang, J.; Ismach, A. F.; Johnston-Halperin, E.; Kuno, M.; Plashnitsa, V. V.; Robinson, R. D.; Ruoff, R. S.; Salahuddin, S.; Shan, J.; Shi, L.; Spencer, M. G.; Terrones, M.; Windl, W.; Goldberger, J. E. *ACS Nano* **2013**, *7*, 2898.
(3) Frank, O.; Dresselhaus, M. S.; Kalbac, M. *Acc. Chem. Res.* **2015**, *48*, 111.
(4) Chhowalla, M.; Shin, H. S.; Eda, G.; Li, L.-J.; Loh, K. P.; Zhang, H. *Nat. Chem.* **2013**, *5*, 263.
(5) Bissett, M. A.; Tsuji, M.; Ago, H. *Phys. Chem. Chem. Phys.* **2014**, *16*, 11124.
(6) Fiori, G.; Bonaccorso, F.; Iannaccone, G.; Palacios, T.; Neumaier, D.; Seabaugh, A.; Banerjee, S. K.; Colombo, L. *Nat. Nanotechnol.* **2014**, *9*, 768.
(7) Miro, P.; Audiffred, M.; Heine, T. *Chem. Soc. Rev.* **2014**, *43*, 6537.
(8) Mak, K.; Lee, C.; Hone, J.; Shan, J.; Heinz, T. *Phys. Rev. Lett.* **2010**, *105*, 136805.
(9) Bertolazzi, S.; Brivio, J.; Kis, A. *ACS Nano* **2011**, *5*, 9703.
(10) Castellanos-Gomez, A.; Poot, M.; Steele, G. A.; van der Zant, H. S. J.; Agraït, N.; Rubio-Bollinger, G. *Adv. Mater.* **2012**, *24*, 772.
(11) Feng, J.; Qian, X.; Huang, C.-W.; Li, J. *Nat. Photonics* **2012**, *6*, 866.
(12) Li, Y.; Li, Y.-L.; Araujo, C. M.; Luo, W.; Ahuja, R. *Catal. Sci. Technol.* **2013**, *3*, 2214.
(13) Castellanos-Gomez, A.; Roldán, R.; Cappelluti, E.; Buscema, M.; Guinea, F.; van der Zant, H. S. J.; Steele, G. A. *Nano Lett.* **2013**, *13*, 5361.
(14) Conley, H. J.; Wang, B.; Ziegler, J. I.; Haglund, R. F.; Pantelides, S. T.; Bolotin, K. I. *Nano Lett.* **2013**, *13*, 3626.
(15) Dou, X.; Ding, K.; Jiang, D.; Sun, B. *ACS Nano* **2014**, *8*, 7458.
(16) Espejo, C.; Rangel, T.; Romero, A.; Gonze, X.; Rignanese, G. M. *Phys. Rev. B* **2013**, *87*, 245114.
(17) Guo, H.; Lu, N.; Wang, L.; Wu, X.; Zeng, X. C. *J. Phys. Chem. C* **2014**, *118*, 7242.
(18) Guzman, D. M.; Strachan, A. *J. Appl. Phys.* **2014**, *115*, 243701.
(19) He, K.; Poole, C.; Mak, K. F.; Shan, J. *Nano Lett.* **2013**, *13*, 2931.
(20) Chang, C.-H.; Fan, X.; Lin, S.-H.; Kuo, J.-L. *Phys. Rev. B* **2013**, *88*, 195420.
(21) Jiang, J.-W. *Nanoscale* **2014**, *6*, 8326.
(22) Li, J.; Medhekar, N. V.; Shenoy, V. B. *J. Phys. Chem. C* **2013**, *117*, 15842.
(23) Li, T. *Phys. Rev. B* **2012**, *85*, 235407.
(24) Nayak, A. P.; Pandey, T.; Voiry, D.; Liu, J.; Moran, S. T.; Sharma, A.; Tan, C.; Chen, C.-H.; Lee, L.-J.; Chhowalla, M.; Lin, J.-F.; Singh, A. K.; Akinwande, D. *Nano Lett.* **2015**, *15*, 346.
(25) Peelaers, H.; Van de Walle, C. *Phys. Rev. B* **2012**, *86*, 241401.
(26) Rice, C.; Young, R.; Zan, R.; Bangert, U.; Wolverson, D.; Georgiou, T.; Jalil, R.; Novoselov, K. *Phys. Rev. B* **2013**, *87*, 081307.
(27) Scalise, E.; Houssa, M.; Pourtois, G.; Afanas'ev, V.; Stesmans, A. *Nano Res.* **2012**, *5*, 43.
(28) Zhu, C.; Wang, G.; Liu, B.; Marie, X.; Qiao, X.; Zhang, X.; Wu, X.; Fan, H.; Tan, P.; Amand, T.; Urbaszek, B. *Phys. Rev. B* **2013**, *88*, 121301.

DOI: 10.1021/acs.nanolett.5b00229
Nano Lett. 2015, 15, 3139−3146

(29) Ashok, K.; Ahluwalia, P. K. *Modell. Simul. Mater. Sci. Eng.* **2013**, *21*, 065015.
(30) Bhattacharyya, S.; Singh, A. *Phys. Rev. B* **2012**, *86*, 075454.
(31) Nayak, A. P.; Bhattacharyya, S.; Zhu, J.; Liu, J.; Wu, X.; Pandey, T.; Jin, C.; Singh, A. K.; Akinwande, D.; Lin, J.-F. *Nat. Commun.* **2014**, *5*, 3731.
(32) Peelaers, H.; Van de Walle, C. G. *J. Phys. Chem. C* **2014**, *118*, 12073.
(33) Hui, Y. Y.; Liu, X.; Jie, W.; Chan, N. Y.; Hao, J.; Hsu, Y.-T.; Li, L.-J.; Guo, W.; Lau, S. P. *ACS Nano* **2013**, *7*, 7126.
(34) Yang, L.; Cui, X.; Zhang, J.; Wang, K.; Shen, M.; Zeng, S.; Dayeh, S. A.; Feng, L.; Xiang, B. *Sci. Rep.* **2014**, *4*, 5649.
(35) Livneh, T.; Sterer, E. *Phys. Rev. B* **2010**, *81*, 195209.
(36) Aksoy, R.; Ma, Y.; Selvi, E.; Chyu, M. C.; Ertas, A.; White, A. *J. Phys. Chem. Solids* **2006**, *67*, 1914.
(37) Chi, Z.-H.; Zhao, X.-M.; Zhang, H.; Goncharov, A. F.; Lobanov, S. S.; Kagayama, T.; Sakata, M.; Chen, X.-J. *Phys. Rev. Lett.* **2014**, *113*, 036802.
(38) Qiu, D.; da Jornada, F.; Louie, S. *Phys. Rev. Lett.* **2013**, *111*, 216805.
(39) Gołasa, K.; Grzeszczyk, M.; Leszczyński, P.; Faugeras, C.; Nicolet, A. A. L.; Wysmołek, A.; Potemski, M.; Babiński, A. *Appl. Phys. Lett.* **2014**, *104*, 092106.
(40) Pimenta, M. A.; del Corro, E.; Carvalho, B. R.; Fantini, C.; Malard, L. M. *Acc. Chem. Res.* **2014**, *48*, 41.
(41) Ribeiro-Soares, J.; Almeida, R. M.; Barros, E. B.; Araujo, P. T.; Dresselhaus, M. S.; Cançado, L. G.; Jorio, A. *Phys. Rev. B* **2014**, *90*, 115438.
(42) Frey, G.; Tenne, R.; Matthews, M.; Dresselhaus, M.; Dresselhaus, G. *Phys. Rev. B* **1999**, *60*, 2883.
(43) Fan, J.-H.; Gao, P.; Zhang, A.-M.; Zhu, B.-R.; Zeng, H.-L.; Cui, X.-D.; He, R.; Zhang, Q.-M. *J. Appl. Phys.* **2014**, *115*, 053527.
(44) Livneh, T.; Spanier, J. E. A Comprehensive Multiphonon Spectral Analysis in MoS_2. 2015, arXiv:1408.6748.
(45) Sekine, T.; Uchinokura, K.; Nakashizu, T.; Matsuura, E.; Yoshizaki, R. *J. Phys. Soc. Jpn.* **1984**, *53*, 811.
(46) Molina-Sánchez, A.; Wirtz, L. *Phys. Rev. B* **2011**, *84*, 155413.
(47) Stacy, A. M.; Hodul, D. T. *J. Phys. Chem. Solids* **1985**, *46*, 405.
(48) Connell, G. A. N.; Wilson, J. A.; Yoffe, A. D. *J. Phys. Chem. Solids* **1969**, *30*, 287.
(49) del Corro, E.; Terrones, H.; Elias, A.; Fantini, C.; Feng, S.; Nguyen, M. A.; Mallouk, T. E.; Terrones, M.; Pimenta, M. A. *ACS Nano* **2014**, *8*, 9629.
(50) Buscema, M.; Steele, G.; van der Zant, H. J.; Castellanos-Gomez, A. *Nano Res.* **2014**, *7*, 561.
(51) Dhakal, K. P.; Duong, D. L.; Lee, J.; Nam, H.; Kim, M.; Kan, M.; Lee, Y. H.; Kim, J. *Nanoscale* **2014**, *6*, 13028.
(52) Sercombe, D.; Schwarz, S.; Pozo-Zamudio, O. D.; Liu, F.; Robinson, B. J.; Chekhovich, E. A.; Tartakovskii, I. I.; Kolosov, O.; Tartakovskii, A. I. *Sci. Rep.* **2013**, *3*, 3489.
(53) Scheuschner, N.; Ochedowski, O.; Kaulitz, A.-M.; Gillen, R.; Schleberger, M.; Maultzsch, J. *Phys. Rev. B* **2014**, *89*, 125406.
(54) McDevitt, N. T.; Zabinski, J. S.; Donley, M. S. *Thin Solid Films* **1994**, *240*, 76.
(55) Kam, K. K.; Parkinson, B. A. *J. Phys. Chem.* **1982**, *86*, 463.
(56) Chakraborty, B.; Matte, H. S. S. R.; Sood, A. K.; Rao, C. N. R. *J. Raman Spectrosc.* **2013**, *44*, 92.
(57) Li, H.; Wu, J.; Huang, X.; Yin, Z.; Liu, J.; Zhang, H. *ACS Nano* **2014**, *8*, 6563.
(58) Loubeyre, P.; Occelli, F.; LeToullec, R. *Nature* **2002**, *416*, 613.
(59) del Corro, E.; Izquierdo, J. G.; González, J.; Taravillo, M.; Baonza, V. G. *J. Raman Spectrosc.* **2013**, *44*, 758.
(60) Kresse, G.; Furthmüller, J. *Phys. Rev. B* **1996**, *54*, 11169.
(61) Blöchl, P. *Phys. Rev. B* **1994**, *50*, 17953.
(62) Kresse, G.; Joubert, D. *Phys. Rev. B* **1999**, *59*, 1758.
(63) Perdew, J.; Burke, K.; Ernzerhof, M. *Phys. Rev. Lett.* **1996**, *77*, 3865.
(64) Monkhorst, H.; Pack, J. *Phys. Rev. B* **1976**, *13*, 5188.
(65) Böker, T.; Severin, R.; Müller, A.; Janowitz, C.; Manzke, R.; Voß, D.; Krüger, P.; Mazur, A.; Pollmann, J. *Phys. Rev. B* **2001**, *64*, 235305.

DOI: 10.1021/acs.nanolett.5b00229
Nano Lett. 2015, 15, 3139−3146